Journal of Alloys and Compounds 502 (2010) 163–168

Contents lists available at ScienceDirect

Journal of Alloys and Compounds

journal homepage: www.elsevier.com/locate/jallcom

Electrical properties of low temperature sintered copper and titanium-codoped copper zinc ferrites

Hsing-I. Hsiang[a,*], Li-Then Mei[a], Chi-Shiung Hsi[b], Yi-Lang Liu[a], Fu-Su Yen[a]

[a] Particulate Materials Research Center, Department of Resources Engineering, National Cheng Kung University, Tainan, Taiwan, ROC
[b] Department of Materials Science and Engineering, National United University, Miaoli, Taiwan, ROC

ARTICLE INFO

Article history:
Received 12 November 2009
Received in revised form 15 April 2010
Accepted 17 April 2010
Available online 15 May 2010

Keywords:
Copper zinc ferrites
NiCuZn ferrites
Electrical properties
Dielectric properties
Cofiring

ABSTRACT

The effects of Cu and Ti substitution on the sintering behavior, substitution mechanism, resistivity and dielectric properties of CuZn ferrites were investigated. Codoped Cu^{2+} and Ti^{4+} can effectively reduce the densification temperature of copper zinc ferrite to below 900 °C and improve the resistivity and dielectric properties. The copper and titanium-codoped CuZn ferrites and NiCuZn ferrites exhibited excellent compatibilities in physical and chemical matching during cofiring. Therefore, the copper and titanium-codoped CuZn ferrites can be a good candidate material for an effective intermediate nonmagnetic layer for NiCuZn ferrites in preparing a multilayer chip inductor with a high rated current.

1. Introduction

Nonmagnetic ferrites such as Zn ferrite and CuZn ferrite have been widely used in the electronics industry [1,2]. Recently, multilayer chip LC filters have been developed as a promising electromagnetic interference (EMI) device [3,4]. They are made with a cofired multilayer structure of ferrite, dielectric and internal conductors. One of the most important processes in manufacturing defect-free multilayer chip LC devices involves capacitor and inductor materials cofiring at a low temperature. Mismatched densification kinetics and severe chemical reactions between the different materials could generate undesirable defects such as delamination, cracks and camber in the final products [5–7]. Nakano et al. [8] reported that a nonmagnetic CuZn ferrite can act as an intermediate layer at the interface between the dielectric and NiCuZn ferrite layer to prevent the above defects in multilayer chip LC devices. The inductance value in a multilayer chip inductor quickly declines as the current exceeds the rated current (DC superposition characteristic). This is caused by the magnetic saturation due to the closed magnetic path in the magnetic body. Tsuzuki [9] reported that an excellent DC superposition characteristic can be obtained when a nonmagnetic ferrite (CuZn ferrite) layer is sandwiched between the NiCuZn ferrite layers. For electronic application, it is important for a nonmagnetic ferrite (zinc ferrite) to be densified at a low temperature and have a high insulation resistivity.

Many researchers [10–12] observed that the addition of Cu can effectively decrease the densification temperature of NiZn ferrite. Rao et al. [13] investigated the influence of the Ti substitution concentration on the DC resistivity and dielectric properties of NiZn ferrite and observed that the resistivity increased with increasing Ti^{4+} ion addition. In our previous study [14], the effects of Cu and Ti substitution on the sintering behavior, electric properties of $(Zn)(Cu_xTi_xFe_{1.98-2x})O_{3.97}$ were investigated and observed that codoped Cu^{2+} and Ti^{4+} can effectively promote zinc ferrite densification and obtain a highest resistivity at $x = 0.05$. However, the densification temperatures of $(Zn)(Cu_xTi_xFe_{1.98-2x})O_{3.97}$ ceramic at $x = 0$–0.1 must be greater than 950 °C, which limits its application on the low temperature cofired ceramic devices. In this study, the content of Cu in the zinc ferrites is increased to promote the densification at below 900 °C and the effects of x values on the sintering behavior, substitution mechanism, resistivity and dielectric properties of $(Zn_{0.8}\ Fe_{0.2})(Cu_{0.2+x}Ti_xFe_{1.78-2x})O_{3.97}$ were investigated using X-ray diffractometer (XRD), scanning electron microscopy (SEM), and dilatometer. Moreover, the cofiring behavior and interfacial interaction between $(Zn_{0.8}Fe_{0.2})(Cu_{0.22}Ti_{0.02}Fe_{1.74})O_{3.97}$/NiCuZn ferrites at 900 °C were studied. Through these investigations an effective intermediate nonmagnetic layer for NiCuZn ferrites in preparing a multilayer chip inductor with a high rated current could be suggested.

* Corresponding author. Tel.: +886 6 2757575x62821; fax: +886 6 2380421.
E-mail address: hsingi@mail.ncku.edu.tw (H.-I. Hsiang).

0925-8388/$ – see front matter © 2010 Elsevier B.V. All rights reserved.
doi:10.1016/j.jallcom.2010.04.134

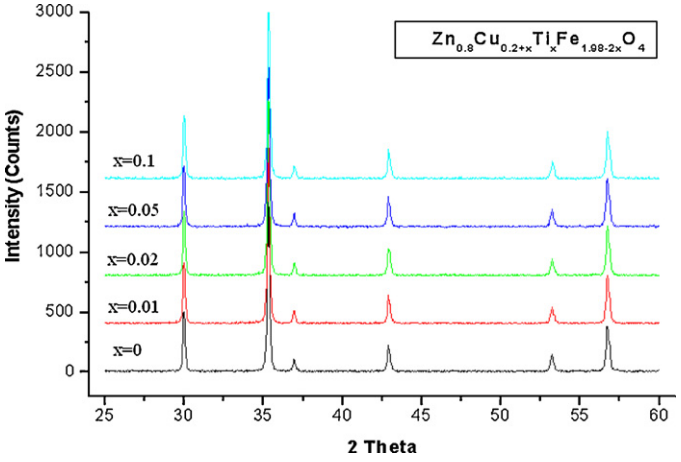

Fig. 1. XRD patterns for the general formula $(Zn_{0.8}Fe_{0.2})(Cu_{0.2+x}\ Ti_xFe_{1.78-2x})O_{3.97}$ ferrite samples with various x values.

2. Experimental

Ferrite powders of composition $(Zn_{0.8}Fe_{0.2})(Cu_{0.2+x}Ti_xFe_{1.78-2x})O_{3.97}$ with $x = 0$–0.1 were prepared from reagent-grade ZnO, CuO, TiO_2 and Fe_2O_3, mixed and then calcined at 750 °C for 2 h. The powders were then milled for 24 h using Y-TZP balls. The powders were dried in an oven and PVA was then added for granulation. The powders were compacted using a cold isostatic press at 150 MPa. These specimens were then debindered at 500 °C and sintered at 900 °C for 2 h. Thermal shrinkage was measured using a dilatometer (Netzsch, DIL 420C). The densities of the sintered samples were determined using the Archimedean method. The CuZn ferrite/NiCuZn ferrite composites were prepared by the sheet method. The NiCuZn ferrites (Ni:Cu:Zn:Fe = 0.58:0.12:0.3:1.98) were prepared from reagent-grade NiO, CuO, ZnO and Fe_2O_3, which were mixed and then calcined at 740 °C for 2 h. The calcined NiCuZn ferrite powders were then milled in a polyethylene bottle with YTZ balls for 24 h in an ethanol medium. For slurry preparation, NiCuZn and $(Zn_{0.8}Fe_{0.2})(Cu_{0.22}Ti_{0.02}Fe_{1.74})O_{3.97}$ ferrite powders were mixed with commercial organic vehicle (MSI 73210). Green sheets were prepared using tape casting method. The green sheets of CuZn and NiCuZn ferrites were hot-isostatic laminated under a pressure of 4000 psi and held at 70 °C for 10 min and then cut into chips of size "0805" (EIA Code 0.08 in. × 0.05 in.). Binder burnout was carried out at 450 °C for 12 h. The composites were sintered at 900 °C for 2 h. The microstructure was observed using scanning electron microscopy (Hitachi, S4100) and the distribution of elements was measured using electron probe microanalysis (EPMA) (JEOL, JXA-8900R). The crystalline phase identification was determined using X-ray diffractometry (Siemens, D5000) with CuK_α radiation. The electrical resistivity of the samples was measured using the two-probe dc technique (Keithley, Multimeter-2001). Dielectric constant was measured using a HP4284A LCR meter over a frequency range of 100 Hz to 1 MHz.

3. Results and discussion

Fig. 1 shows the XRD patterns for the general formula $(Zn_{0.8}Fe_{0.2})(Cu_{0.2+x}Ti_xFe_{1.78-2x})O_{3.97}$ ferrite samples with various x values. For samples with $x = 0$–0.1, the crystalline structure remained a cubic spinel structure with no other phases observed.

The variation in the lattice parameter as a function of the x value is shown in Fig. 2. The lattice parameter increased as the x value increased from 0 to 0.01 and then declined slightly as x value increased from 0.02 to 0.1. This is in good agreement with the observation that the lattice parameter of $Cu_{1+x}Ti_xFe_{2-2x}O_4$ increased with increasing x value reported by Patil et al. [15]. In general Cu^{2+} and Ti^{4+} ions have a strong tendency to occupy octahedral sites, while Zn^{2+} ions prefer to occupy tetrahedral sites and Fe^{3+} ions are distributed between the two sites for a spinel structure [16–18]. The ionic radius of Cu^{2+} and Ti^{4+} are both larger than that of Fe^{3+}, which results in the lattice parameter of $(Zn_{0.8}Fe_{0.2})(Cu_{0.2+x}Ti_xFe_{1.78-2x})O_{3.97}$ increasing with increasing x value. Further increase in x value above 0.02, the lattice parameter decreased. This may be explained by the fact that a certain number of Fe^{3+} ions start to occupy tetrahedral sites, which leads

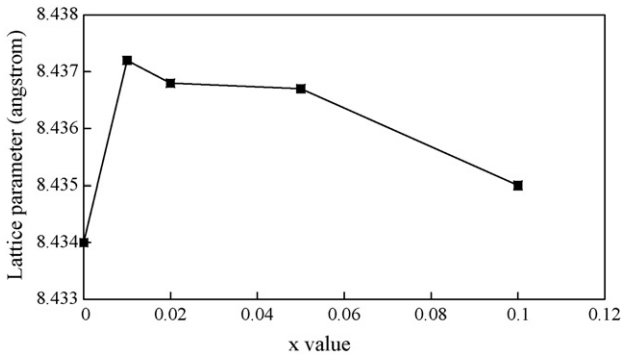

Fig. 2. Variation in the lattice parameter as a function of the x value. The accuracy of lattice parameters was determined to within 0.001 Å.

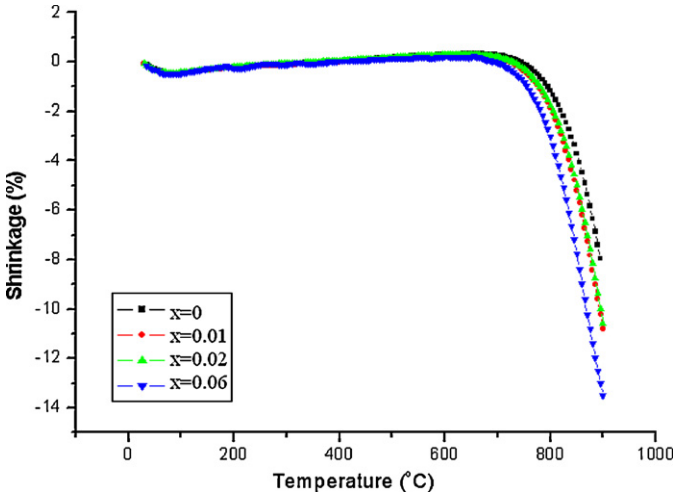

Fig. 3. Dilatometric analyses results of samples with various x values.

to Zn^{2+} ions on the tetrahedral sites being expelled and ZnO precipitation. The replacement of Zn^{2+} ions on the tetrahedral sites by Fe^{3+} ions, which have an ionic radius smaller than that of Zn^{2+} (Fe^{3+}: 0.049 nm, Zn^{2+}: 0.06 nm), results in the decrease in lattice parameter.

Fig. 3 demonstrates that the onset of shrinkage occurring at lower temperatures and larger shrinkages were observed for samples with larger x values. The relative densities of samples with various x values sintered at 900 °C are shown in Fig. 4. With the exception of samples with $x = 0$, the relative densities for all samples reached above 90%. Note that the relative densities increased as the x value increased from 0 to 0.05 and then declined slightly as x value were increased to 0.1. These results indicate that codoped

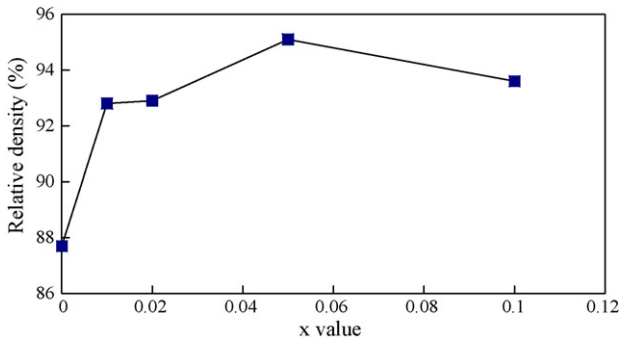

Fig. 4. Relative densities of samples with various x values sintered at 1000 °C.

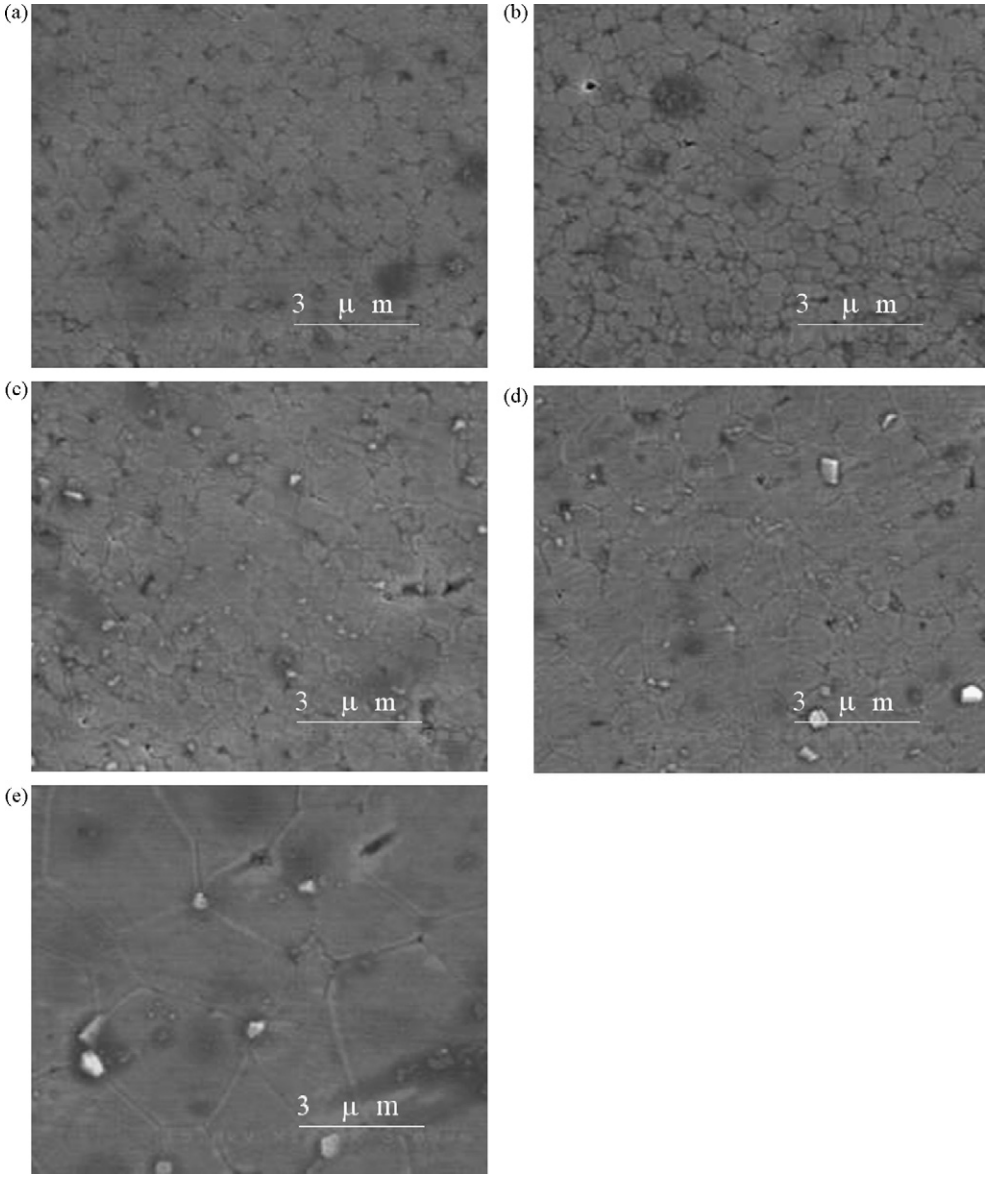

Fig. 5. Microstructures of samples with various x values sintered at 900 °C (a) $x = 0$, (b) $x = 0.01$, (c) $x = 0.02$, (d) $x = 0.05$, (e) $x = 0.1$.

Cu^{2+} and Ti^{4+} can effectively reduce the densification temperature of copper zinc ferrite to below 900 °C.

Fig. 5 shows the microstructures of samples with various x values sintered at 900 °C. For the samples with x values = 0–0.05, the grain sizes are all about 0.3–1 μm and the grain sizes increased to about 1–3 μm as x value was increased to 0.1. Secondary phase precipitates existing mainly in the triple junctions were observed in the samples with x value higher than 0.02. The precipitates can be identified as Zn-rich phase on the basis of EDS result (atomic ratio of Fe:Cu:Zn = 32.33:4.03:63.64).

The electric resistivity of the samples with various x values measured at room temperature is shown in Fig. 6. Initially, the resistivity increased rapidly as the x value was increased from 0 to 0.01. The decrease in resistivity was observed as the x value was increased to 0.1. The change in resistivity with x value can be explained by the Verwey mechanism, which consists of electron exchanges between ions having multiple valence states at equivalent crystallographic sites, such as the electron exchange between Fe^{2+} and Fe^{3+} ions on octahedral sites. For samples with $x = 0.01$, Cu^{2+} and Ti^{4+} ions dissolved into the spinel structure and mainly occupied the octahedral sites, which led to the substitution of Fe^{3+} ions. The substitution ions, Cu^{2+} and Ti^{4+} ions, which do not participate in the electronic exchange dilute the Fe^{2+} and Fe^{3+} ion concentration on octahedral sites and also hinder electron hopping between Fe^{2+} and Fe^{3+} ions, which leads to the increase in resistivity [19]. As x value increased

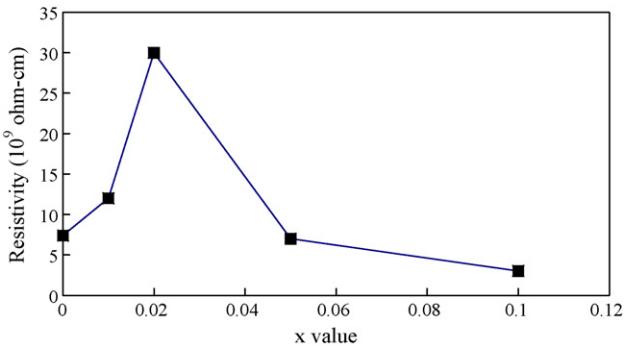

Fig. 6. Electric resistivity of samples with various x values measured at room temperature.

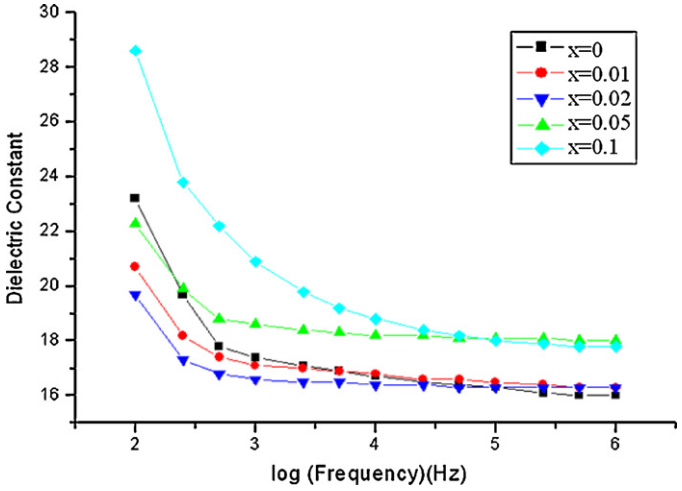

Fig. 7. Variation in dielectric constant for samples with various x values as a function of frequency.

up to 0.02, the occurrence of low resistivity phase, Zn-rich phase, at grain boundary (Fig. 5) was observed, which may lead to the decrease in the resistivity [20].

The variations in dielectric constant for samples with various x values as a function of frequency are shown in Fig. 7. For the sample with $x = 0$, the dielectric constant decreased rapidly with increasing frequency up to 10 kHz and beyond that remained constant. A barrier–layer structure with semiconducting areas encircled by insulating layers can be used to explain the very large dielectric constant of zinc ferrite ($x = 0$) at low frequency. This behavior is characterized by the space charge polarization arising from differences between the conductivity of the various phases present. At low frequency electron hopping occurs between Fe^{3+} and Fe^{2+} on the octahedral sites. The electrons reach the grain boundary through hopping and are piled up at the grain boundaries, which results in the interfacial polarization. However, as the frequency is increased, the probability of electrons reaching the grain boundary decreases, which results in a decrease in the interfacial polarization [19]. Therefore, the dielectric constant decreases with increasing frequency. As the x value increased (up to 0.02), the resistivity increased, which leads to the decrease in space charge polarization. Therefore, the slope of the dielectric constant variation with frequency decreased as the x value increased (up to 0.02). As the

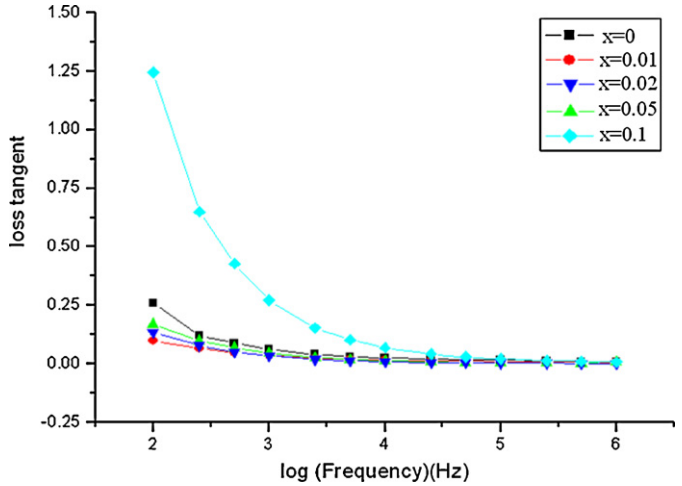

Fig. 8. Variation in dielectric loss for samples with various x values as a function of frequency.

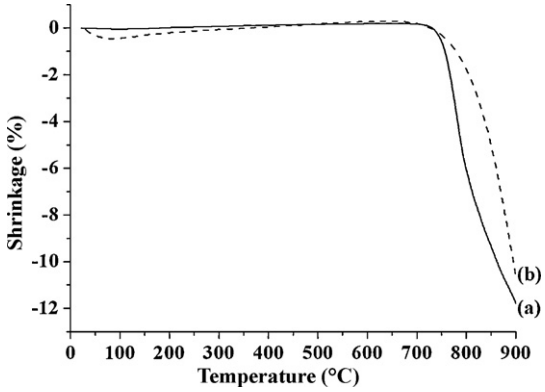

Fig. 9. Shrinkage curves of (a) NiCuZn ferrites and (b) $(Zn_{0.8}Fe_{0.2})(Cu_{0.22}Ti_{0.02}Fe_{1.74})O_{3.97}$ ferrites.

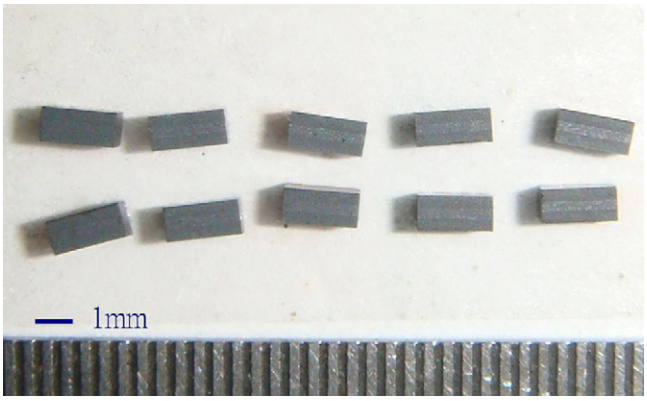

Fig. 10. Side-view of the 0805 chips with codoped CuZn ferrites sandwiched between NiCuZn ferrites sintered at 900 °C for 2 h.

x value increased ($x \geqq 0.05$), the resistivity declined significantly resulting in an increase in the amount of space charges existing in the grains, which leads to the increase in the interfacial polarization.

The variations in dielectric loss for samples with various x values as a function of frequency are shown in Fig. 8. It shows that the dielectric loss at low frequency decreased as the x value increased from 0 to 0.05, and then increased significantly as x value increased

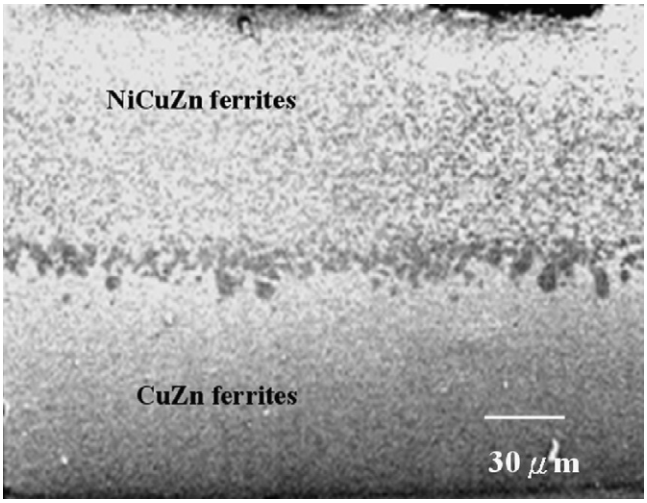

Fig. 11. Cross-sectional view of the interface between NiCuZn and $(Zn_{0.8}Fe_{0.2})(Cu_{0.22}Ti_{0.02}Fe_{1.74})O_{3.97}$ ferrites cofired at 900 °C for 2 h.

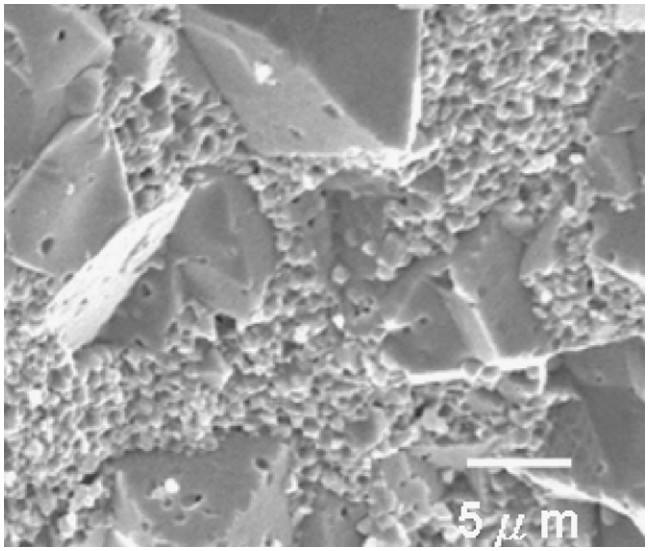

Fig. 12. Larger magnification SEM micrographs of the interface between NiCuZn and $(Zn_{0.8}Fe_{0.2})(Cu_{0.22}Ti_{0.02}Fe_{1.74})O_{3.97}$ ferrites cofired at 900 °C for 2 h.

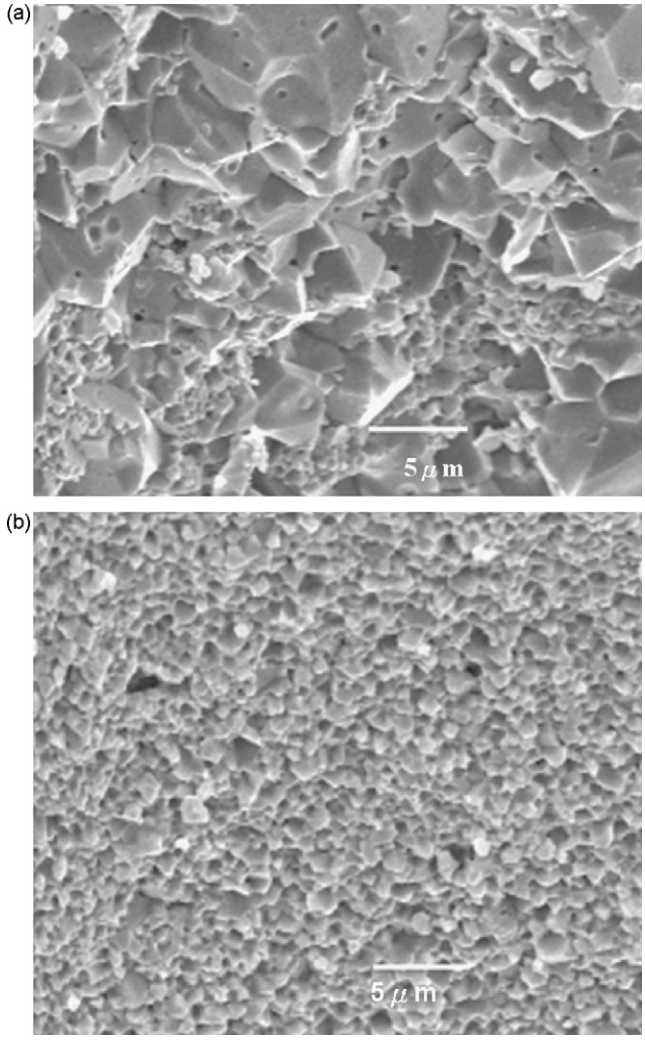

Fig. 13. Microstructures of the ferrites on the top and bottom of the composites (a) NiCuZn ferrites; (b) $(Zn_{0.8}Fe_{0.2})(Cu_{0.22}Ti_{0.02}Fe_{1.74})O_{3.97}$ ferrites.

to 0.1, which can be accounted for the dielectric loss at low frequency resulted from the space charge polarization.

The shrinkage curves of NiCuZn and $(Zn_{0.8}Fe_{0.2})(Cu_{0.22}Ti_{0.02}Fe_{1.74})O_{3.97}$ ferrites are shown in Fig. 9, indicating that the NiCuZn ferrites shrinkage behavior is quite well matched with $(Zn_{0.8}Fe_{0.2})(Cu_{0.22}Ti_{0.02}Fe_{1.74})O_{3.97}$ ferrites. Fig. 10 shows the side-view of the 0805 chips with codoped CuZn ferrites sandwiched between NiCuZn ferrites sintered at 900 °C for 2 h. It indicates that the chips are free of any warpage due to the similar shrinkage behaviors of codoped CuZn ferrites and NiCuZn ferrites. Fig. 11 shows the cross-sectional view of the interface between NiCuZn and $(Zn_{0.8}Fe_{0.2})(Cu_{0.22}Ti_{0.02}Fe_{1.74})O_{3.97}$ ferrites cofired at 900 °C for 2 h. No visible delamination or gap was observed between the interfaces. The larger magnification SEM micrograph of the interface between NiCuZn and $(Zn_{0.8}Fe_{0.2})(Cu_{0.22}Ti_{0.02}Fe_{1.74})O_{3.97}$ ferrites cofired at 900 °C for 2 h is shown in Fig. 12. It indicates that the occurrence of the interpenetration of the NiCuZn and $(Zn_{0.8}Fe_{0.2})(Cu_{0.22}Ti_{0.02}Fe_{1.74})O_{3.97}$ particles at the interface due to the lamination process [21] and the grain sizes of the NiCuZn and $(Zn_{0.8}Fe_{0.2})(Cu_{0.22}Ti_{0.02}Fe_{1.74})O_{3.97}$ ferrites near the interface were nearly same as those of the ferrites on the top and bottom of the composites and no second phase was observed (Fig. 13). It indicates that excellent compatibility in physical and chemical matching between NiCuZn and $(Zn_{0.8}Fe_{0.2})(Cu_{0.22}Ti_{0.02}Fe_{1.74})O_{3.97}$ ferrites.

4. Conclusions

A nonmagnetic ferrite, $(Zn)(Cu_xTi_xFe_{1.98-2x})O_{3.97}$, with high insulation resistance was developed in this work. The codoped Cu^{2+} and Ti^{4+} can effectively reduce the densification temperature of copper zinc ferrite to below 900 °C. In samples with $x = 0.01–0.02$, Cu^{2+} and Ti^{4+} ions dissolved into the spinel structure and occupied mainly the octahedral sites, resulting in an increase in resistivity. However, as the x value increased above 0.1, the resistivity decreased rapidly due to the occurrence of a large amount of Zn-rich precipitates in the triple junctions. The dielectric responses of these samples can be described using an interfacial polarization model. Increasing the resistivity due to the Cu and Ti-codoping in zinc ferrite resulted in a decrease in the amount of space charges existing in the grains, leading to a decrease in the space charge polarization. The interfaces between the CuZn and NiCuZn ferrites layers after cofiring were free of delamination or cross-diffusion, indicating that the copper and titanium-codoped CuZn ferrites and NiCuZn ferrites exhibited excellent compatibilities in physical and chemical matching during cofiring. Therefore, the copper and titanium-codoped CuZn ferrites can be a good candidate material for an effective intermediate nonmagnetic layer for NiCuZn ferrites in preparing a multilayer chip inductor with a high rated current.

Acknowledgment

This work was financially co-sponsored by the Ministry of Economic Affairs of the Republic of China through contract (97-EC-17-A-08-S1-023) and National Science Council of the Republic of China (NSC98-2221-E-006-077-MY3).

References

[1] P. Uniyal, K.L. Yadav, J. Alloys Compd. 492 (2010) 406–410.
[2] M.A. Elkestawy, J. Alloys Compd. 492 (2010) 616–620.
[3] H.M. Sung, C.J. Chen, L.J. Wang, W.S. Ko, IEEE Trans. Mag. 34 (1998) 1363–1365.
[4] X. Liu, F. Gao, J. Liu, C. Tian, J. Alloys Compd. 470 (2009) 269–272.
[5] H.I. Hsiang, W.C. Liao, Y.J. Wang, Y.F. Cheng, J. Eur. Ceram. Soc. 24 (2004) 2015–2021.
[6] J.H. Jean, C.R. Chang, J. Am. Ceram. Soc. 80 (1997) 3084–3092.
[7] X. Liu, F. Gao, C. Tian, J. Alloys Compd. 486 (2009) 743–746.
[8] A. Nakano, S. Saito, T. Nomura, US Patent 5476728 (1995).

[9] K. Tsuzuki, Eur. Patent 1739695 (2007).
[10] T.T. Ahmed, I.Z. Rahman, M.A. Rahman, J. Mater. Process. Technol. 153–154 (2004) 797–803.
[11] H. Su, H. Zhang, X. Tang, B. Liu, Z. Zhong, J. Alloys Compd. 475 (2009) 683–685.
[12] H. Su, H. Zhang, X. Tang, Z. Zhong, Y. Jing, Mater. Sci. Eng. B 162 (2009) 22–25.
[13] B.P. Rao, K.H. Rao, T.V. Rao, A. Paduraru, O.F. Caltun, J. Opt. Adv. Mater. 7 (2005) 704–710.
[14] H.I. Hsiang, Y.L. Liu, J. Alloys Compd. 472 (2009) 516–520.
[15] B.L. Patil, S.R. Sawant, S.A. Patil, Phys. Status Solidi A 133 (1992) 147–152.
[16] E.J.W. Verwey, E.L. Heilmann, J. Chem. Phys. 15 (1947) 174–180.
[17] B.A. Wechsler, D.H. Lindsley, C.T. Prewitt, Am. Miner. 69 (1984) 754–770.
[18] A.R. West, Basic Solid State Chemistry, John Wiley & Sons, New York, 1984, pp. 305–315.
[19] K.W. Wagner, Ann. Phys. 40 (1913) 817.
[20] H.A. Daeoud, S.K.K. Shaat, Islamic Univ. J. 14 (2006) 165–182.
[21] H. Hellebrand, Materials Science and Technology, vol. 17A, Processing of ceramics, in: R.J. Brook (Ed.), VCH Publishers Inc., New York, 1996, pp. 189–265.